J Therm Anal Calorim (2017) 128:883–890
DOI 10.1007/s10973-016-5986-5

Thermal analysis and crystallization of the glasses inside the BaO–SrO–TiO_2–$NaPO_3$ system

H. Sinouh[1] · L. Bih[1] · B. Manoun[2,3] · P. Lazor[4]

Received: 5 April 2016 / Accepted: 19 November 2016 / Published online: 19 December 2016

Abstract The $x\mathrm{Ba_{0.5}Sr_{0.5}TiO_3}$–$(1-x)\mathrm{NaPO_3}$ ($x = 0$–0.20 mol%) glasses were prepared by the conventional melt-quenching method. The amorphous state of the samples was verified by X-ray diffraction. The density, molar volume, glass transition temperature (T_g), micro-hardness and the crystallization temperature (T_c) are determined for each glass. It is found that they depend strongly on the chemical composition of the glasses. The results of the micro-hardness show an increase in the H_v parameter with the $Ba_{0.5}Sr_{0.5}TiO_3$ content. The crystallization of glasses is made by submitting samples to heat treatments, and the crystallized phases are identified by XRD. The kinetic of the crystallization is carried out by thermal analysis using DSC technique. The mechanism of crystallization is proposed according to the determined activation energy (E_a) and the Avrami parameter (n). The structural approach of the glasses was realized out by IR spectroscopy. This technique has highlighted the co-existence of different phosphate and titanium structural units in the glassy-matrix.

Keywords Phosphate · Glasses · Glass–ceramics · Crystallization · Kinetic · Thermal analysis

Introduction

The applications of ceramic materials depend on their chemical composition and microstructure. They are, generally, used as traditional and technique ceramics. The advanced ceramics are used in automotive, energy, environment, electronic, mechanical, medical, aerospace applications as well as modern industries. Advanced ceramics are making news across worldwide industry. Electrical and electronic ceramics currently dominate applications. Strontium titanate ($SrTiO_3$) and barium titanate ($BaTiO_3$) have properties that make them attractive in memory devices. For example, the solid solution $Ba_{1-x}Sr_xTiO_3$ is commonly used as a capacitor in DRAMS since these phases have high charge storage densities, low leakage currents and dielectric breakdown sufficient to achieve gigabyte densities [1, 2]. In contrast to polycrystalline ceramics prepared by solid-state mixing and firing, glass–ceramics can achieve low porosity levels and hence high breakdown voltages. Generally, the properties of the glass–ceramics are determined by the main crystallization phases precipitated from the mother glass. So, when developing new kind of glass–ceramics, it is very important to control crystallization of the glasses [3].

Glass–ceramics are composites, consisting of micro- or nano-crystallites embedded in a glass matrix, formed by controlled crystallization of glasses. The rate of nucleation and growth of crystals can be controlled, and hence, the resulting properties of glass–ceramics can be tailored. The perovskite glass–ceramics have attracted the attention of the researchers and scientists due to its application in energy storage devices. These are technologically important class of materials and used in energy storage devices due to its high dielectric constant, low loss and high mechanical strength [4].

✉ L. Bih
bihlahcen@yahoo.fr

[1] Equipe de Physico-Chimie de la Matière Condensée, PCMC, Faculté des Sciences de Meknes, Meknes, Morocco

[2] Univ. Hassan 1er, Laboratoire des Sciences des Matériaux, des Milieux et de la Modélisation (LS3M), 25000 Khouribga, Morocco

[3] Center for Advanced Materials (CAM), Mohammed VI Polytechnic University, Lot 660 Hay Moulay Rachid, 43150 Ben Guerir, Morocco

[4] Department of Earth Sciences, Uppsala University, 752 36 Uppsala, Sweden

The ferroelectric glass–ceramic materials, such as homogeneous mixing of ferroelectric phases with glass, have been utilized in ferroelectric and piezoelectric applications [5, 6]. In the recent years, there have been developments of some new pyroelectric and piezoelectric glass–ceramics [7–9]. However, some applications in electronics require massive pieces of ferroelectric materials with variable dielectric properties and shapes. Such materials could be used to regulate and homogenize fields in microwave furnaces [10], which demand variable permittivity within a wide range and with low dielectric loses [11]. It is to note that all the studied glass–ceramics are based on silicate and/or borosilicate. No or less investigation of the possibility of titanate precipitated in phosphate glass exists in the literature. Attempts to precipitate crystallites in glass ceramics with the aim of obtaining improved properties have not yielded encouraging results in the case of perovskite titanates. If the problems associated with precipitation of crystallites in glass ceramics could be solved, this would greatly enhance the utilization of ferroelectric glass ceramics. In this view, the undertaken work is performed in order to know whether the phosphate glasses could stabilize single or more perovskite crystalline phases.

In the present work, our interest focuses on the study of phosphate glasses inside the $NaPO_3$–$Ba_{0.5}Sr_{0.5}TiO_3$ system. The experimental conditions for the synthesis are determined. Their characterization is performed by density measurements, thermal analysis (DSC), Micro-hardness and Infrared spectroscopy (IR). Their crystallization kinetic is performed using DSC thermal analysis.

Experimental

The $x Ba_{0.5}Sr_{0.5}TiO_3$–$(1 - x)NaPO_3$ glasses with $0 \leq x \leq 0.2$ mol% are prepared by mixing and grinding appropriate contents of vitreous $NaPO_3$ and $Ba_{0.5}Sr_{0.5}TiO_3$ crystalline phase. The glasses are elaborated by the conventional melt-quenching route. Well-mixed powders containing appropriate amounts of the above chemicals were melted at the temperature 1000 °C. The melt is poured into an aluminum mold preheated at 350 °C. The obtained samples are then stored in a vacuum desiccator. The amorphous state of the samples is verified by X-ray diffraction using a Philips X'Pert apparatus equipped with a CuK_{α} X-ray source and a Ni filter ($\lambda_{Cu} = 1.5406$ Å). The crystallization process is realized by submitting the glass samples to heat treatments at 600 °C in air for 3 h.

The density measurements (D) of the glasses are taken by the Archimedes method using diethyl orthophthalate at 25 °C as the suspension medium. The glass density is given by the following equation:

$$\rho = \left[m_a / \left(m_{ort} - m_{ort+glass}\right)\right] \times \rho_{ort} \quad (1)$$

where m_a = mass of the sample (glass) measured in air; m_{ort} = mass of diethyl orthophthalate only; $m_{ort+glass}$ = mass of glass immersed in diethyl orthophthalate; and $\rho_{ort} = 1.11422$ g cm^{-3}.The precision of the measurements taken is estimated to be 0.01 g cm^{-3}. Molar volume (V_m) of each glass is derived from the density and molar weight values:

$$(V_m = M/D) \quad (2)$$

where M is the molecular weight of the glass expressed as the mole fractions of the oxides multiplied by their molecular weights.

The micro-hardness measurements have been taken in the Vickers scale (H_v) with a Leitz apparatus. (H_v) refers to the Vickers hardness. It is defined as the resistance to indentation and is determined by measuring the permanent depth of the indentation. The visualization of the pyramidal stamp has been improved by using a gold coating deposition on the polished surface of the glass sample. The accuracy is ±10 DaN mm^{-2}. From deformation–fracture patterns in Vickers indenter tests, the values of Vickers hardness, H_v, for the glasses were evaluated using the equation $H_v = P/\alpha_0 a^2$ where (P) is an applied load, (a) is a characteristic indentation diagonal and (α_0) is an indenter constant of 2.15 for a diamond pyramid indenter. The measuring conditions are 100 g load at 25 ± 2 °C and 50 ± 5% relative humidity.

The thermal stability of the studied glasses is studied by the differential scanning calorimetry (DSC). DSC runs were carried out for ground glass batches about 130 mg in nitrogen atmosphere using different heating rates from 5 to 20 °C min^{-1} using a DSC 131 Evo analyzer.

The particle size used for DSC is about 50 µm. The glass transition temperature (T_g), the onset crystallization temperature (T_c) and the peak crystallization temperature (T_p) were determined using the software associated to the equipment, and the measurement error is assumed to be 4 °C.

The local structure of the samples was examined by the Fourier transform infrared FTIR TENSOR27 spectrometer. FTIR absorption spectra of all glasses were recorded in the 400–1500 cm^{-1} frequency range at room temperature. For these measurements, each sample was ground to a fine powder, mixed with KBr in the ratio 1:300, and vacuum pressed into a disk.

Results and discussion

XRD analysis

The width of the glassy region inside the system $Ba_{0.5}Sr_{0.5}TiO_3$–$NaPO_3$ is checked by X-ray diffraction analysis and the transparency of the samples. The homogeneous glasses could be elaborated up to 20 mol% of $Ba_{0.5}Sr_{0.5}TiO_3$. XRD patterns for different samples in the range of compositions ($0 < x < 0.20$) show only broad hallo around 25–35° (2θ values), which confirm the amorphous nature of these samples.

Density and molar volume

Results of the density measurements and the calculated molar volume of the studied glasses $x$$Ba_{0.5}Sr_{0.5}TiO_3$–$(1-x)$$NaPO_3$ ($x = 5$, 10, 15 et 20 mol%) are represented in Fig. 1 and listed in Table 1. One can observe that the density and the molar volume increases and decreases, respectively, with the $Ba_{0.5}Sr_{0.5}TiO_3$ content. The substitution of $NaPO_3$ by $Ba_{0.5}Sr_{0.5}TiO_3$ is accompanied with an increase in molecular mass, that is, why probably the density variation shows the increasing trend with $Ba_{0.5}Sr_{0.5}TiO_3$ content. A decrease in the molar volume versus composition parameter (x) could not be interpreted in terms decreasing of the mean ionic radius related to the substitution of ($Na^+ + P^{5+}$) by ($Sr^{2+} + Ti^{4+}$) since $r(Ti^{4+}) = 0.61$ Å, $r(Sr^{2+}) = 1.18$ Å, $r(Na^+) = 1.02$ Å and $r(P^{5+}) = 0.17$ Å [12]. However, the observed decrease in the molar volume versus (x) could be associated to the decreasing number of non-bridging oxygen atoms in the glassy-matrix. In other words, this decrease is due to the decrease in bond length or interatomic spacing among the atoms of glass network which causes closing of the structure in agreement with the fact that when non-bridging oxygen (NBO) is converted to bridging oxygen (BO), the average M–O distance decreases [13–16]. Moreover, the variation $V = f(x)$ suggests the formation of more covalent Sr–O, Ba–O and Ti–O bonds with short lengths, instead of ionic Na–O bonds, which reticules the phosphate network and lead to the close structure of the glasses. The same results were observed in $SrTiO_3$–$NaPO_3$ system [17].

Micro-hardness (H_v)

Values of micro-hardness, H_v, for the glasses $x$$Ba_{0.5}Sr_{0.5}TiO_3$–$(1-x)$$NaPO_3$ are listed in Table 1. It is seen that H_v increases with the increase in titanium content (Fig. 2). This change can be attributed to an increase in the network strength. It is well known that the magnitude of micro-hardness is related to bond energies [18]. According to the chemical composition of the studied glasses, one can consider that P–O–P, P–O–Ti and Ti–O–Ti are the principal covalent bonds which determine the cohesive energies of the network [3]. Therefore, the observed increase in H_v with $Ba_{0.5}Sr_{0.5}TiO_3$ could be explained by the formation of P–O–Ti and/or Ti–O–Ti linkages in their glassy-matrix.

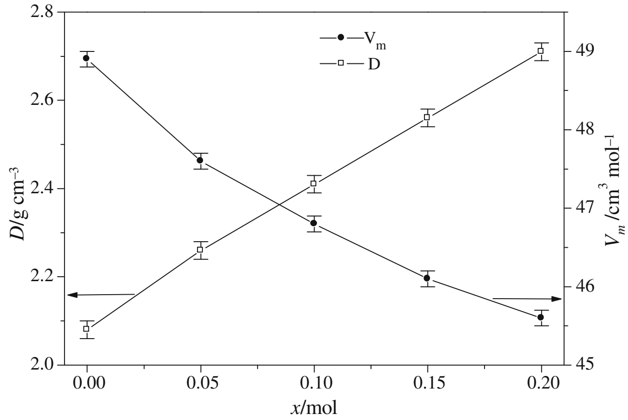

Fig. 1 Density and molar volume as a function of composition (x) for the $x$$Sr_{0.5}Ba_{0.5}TiO_3$–$(1-x)$$NaPO_3$ glasses

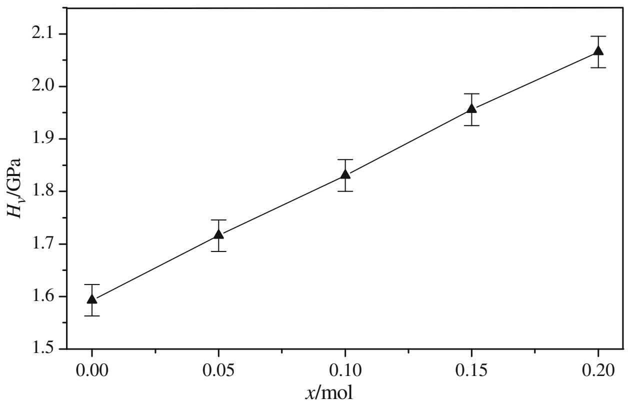

Fig. 2 Variation of the micro-hardness (H_v) as a function of the composition for the glasses. Line is drawn as guide to the eye

Table 1 Some physical properties of the $x$$Ba_{0.5}Sr_{0.5}TiO_3$–$(1-x)$$NaPO_3$ glasses

x	Densité/g cm^3	V_m/cm^3 mol^{-1}	T_g/°C	T_c/°C	T_g–T_c/°C	H_v/GPa
0	2.08	48.9	284	387	103	1.59
0.05	2.26	47.6	390	524	134	1.72
0.1	2.41	46.8	407	544	137	1.81
0.15	2.56	46.1	425	569	144	1.96
0.2	2.71	45.6	430	571	141	2.07

Differential scanning calorimetry

The DSC curves of the glasses studied are shown in Fig. 3. Table 1 shows the value of the glass transition temperature (T_g), the crystallization temperature (T_c) and the value of the parameter (T_c–T_g) of each glass. Figure 4 represents the variation of the glass transition temperature (T_g) as a function of $Ba_{0.5}Sr_{0.5}TiO_3$ content. The substitution of $NaPO_3$ for $Ba_{0.5}Sr_{0.5}TiO_3$ leads to a large increase in T_g in the glass and shows that the structure is strongly strengthened. We assume that in this case, when strontium and titanium cations substitute sodium ions, –P–O…Sr and –P–O… Ti, more covalent bonds are formed instead of ionic Na–O links (the Sr and Ti electronegativities being larger than that of Na). This means that the glasses will show high glass transition temperature. The formation of these energy links could help to improve the cross-linking of the glass network [3]. It is observed that Tg temperature increases rapidly in the composition region $0 \leq x \leq 0.05$. Then, it increases slowly for glasses with $x > 0.05$. The nonlinear increase in temperature T_g in both areas compositions $0 \leq x \leq 0.05$ and $x > 0.05$ suggests that the first introduction of titanium in the network induces a strong strengthening of the glass. Furthermore, the crystallization temperature T_c and the T_c–T_g parameter increase with increasing $Ba_{0.5}Sr_{0.5}TiO_3$ content in the range $0 \leq x \leq 0.15$. These results show an easy verification and high thermal stability of the glasses containing $Ba_{0.5}Sr_{0.5}TiO_3$ [3, 17].

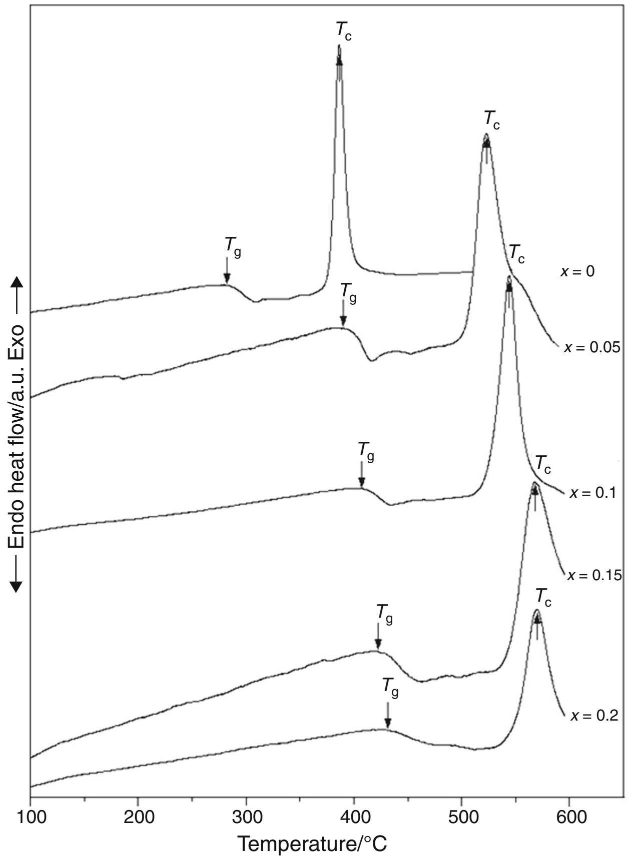

Fig. 3 DSC curves obtained for the $xSr_{0.5}Ba_{0.5}TiO_3$–$(1 - x)$ $NaPO_3$ glasses

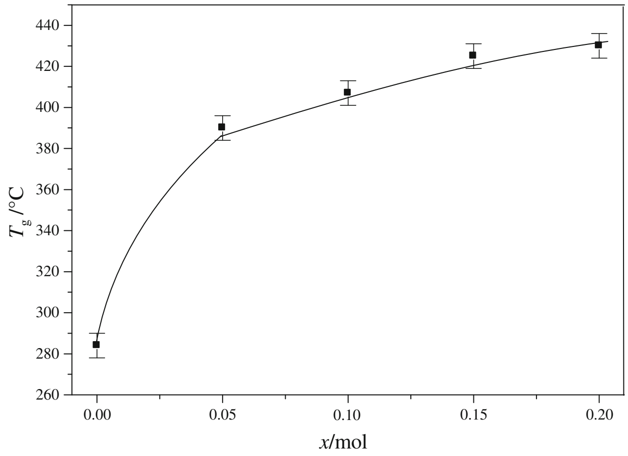

Fig. 4 Composition dependence of the glass transition temperature (T_g)

Crystallization of the glasses

The crystallization is realized by submitting piece of $xBa_{0.5}Sr_{0.5}TiO_3$–$(1 - x)NaPO_3$ glasses to heat treatment at 600 °C for 3 h. Figure 5 shows the obtained XRD patterns for each sample. The analysis of these patterns shows the crystallization of different phases mainly metaphosphate $Sr(PO_3)_2$ (JCPDS 89-6594), pyrophosphates $Ba_2P_2O_7$ (JCPDS 09-0045) and titanate Na_2TiO_3 (JCPDS 37-0345). When the glass composition contains large amount of $Ba_{0.5}Sr_{0.5}TiO_3$ ($x = 20$ mol%), the intensity of peaks relative to the perovskite Na_2TiO_3 phase increases. One can also observe the formation of the $Sr_2P_2O_7$ (JCPDS 12-0362) phase when the content of titanium increases in the sample. It seems that in the glass–ceramics the alkaline-earth elements are preferentially bonded to phosphate structural units while sodium ion reacts with titanate groups.

Crystallization kinetics by DSC

It is well known that the kinetic parameters of the glass crystallization, activation energy (E_c) and Avrami exponent (n) could be determined using different methods [19]. The activation energy for crystallization (E_c), denotes the nucleation behavior in the crystallization process, was determined according to the Kissinger method, considering the heating rate dependence of the peak temperature (T_p) as given in the following relationship [20, 21]:

Fig. 5 XRD patterns of the crystallized glasses at 600 °C for 3 h

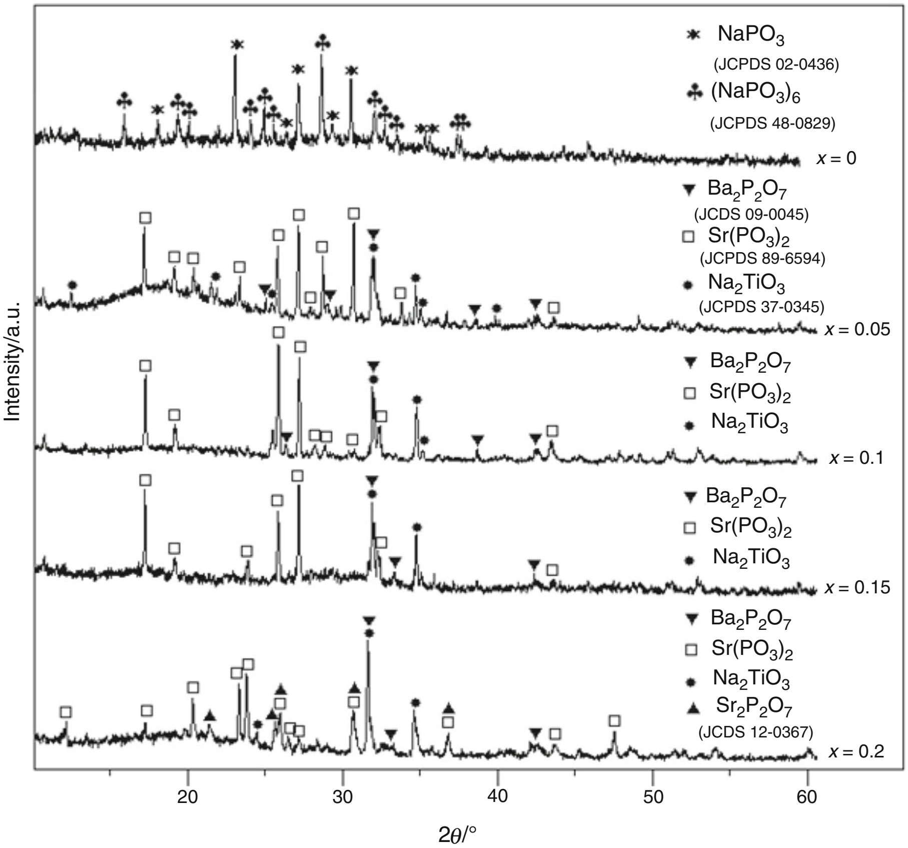

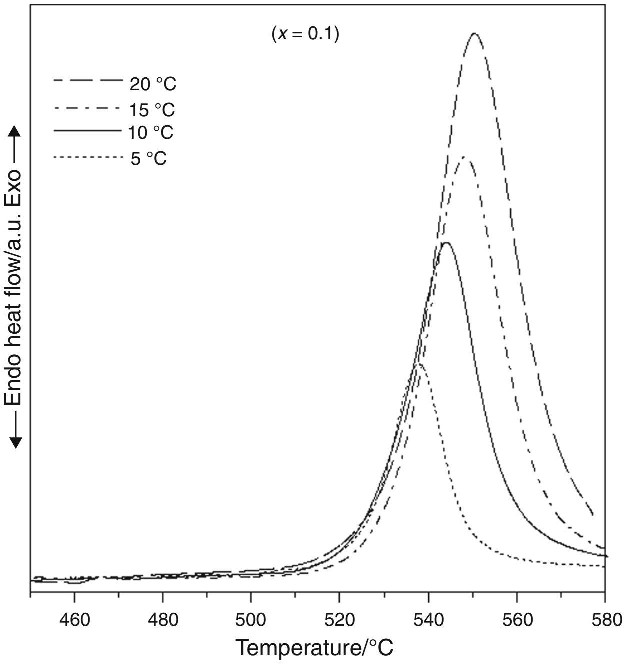

Fig. 6 DSC curves for the glass ($x = 0.1$) under different heating rates

Table 2 Crystallization temperature and Avrami parameter of the glass ($x = 0.1$) at different heat crystallization rates

Glass	β/°C min^{-1}	T_p/°C	βT/°C	Avrami parameter/n
$x = 0.1$	5	538	15	1.72
	10	544	18	1.47
	15	549	20	1.35
	20	551	21	1.29

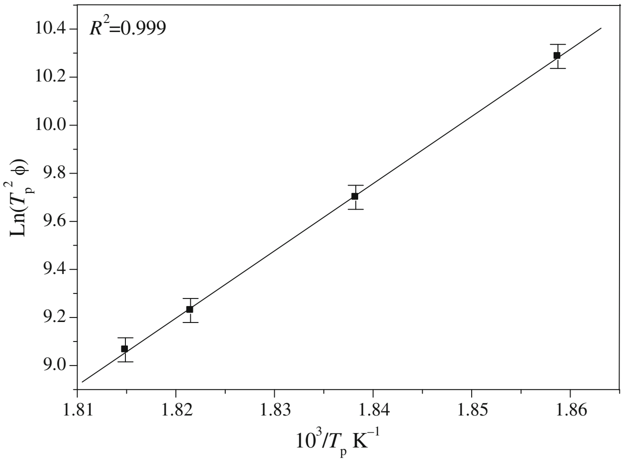

Fig. 7 Plot of ln(T_p^2/β) versus inverse temperature for the glass ($x = 0.1$)

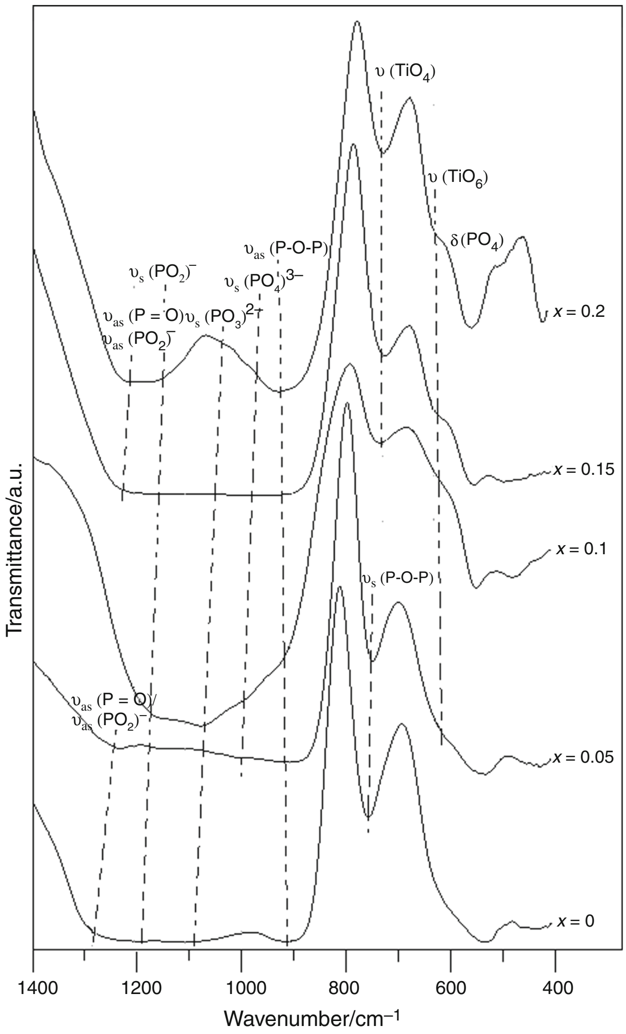

Fig. 8 Infrared spectra of the $x\mathrm{Ba}_{0.5}\mathrm{Sr}_{0.5}\mathrm{TiO}_3$–$(1-x)\mathrm{NaPO}_3$ glasses

$$\ln\left(T_p^2/\beta\right) = E_c/\left(RT_p\right) + \text{constant} \tag{3}$$

where β and R are the heating rate and the universal gas constant, respectively. The same approach is used to study different oxide glassy systems [22–25].

The DSC curves for the glass powder obtained at different heating rates are presented in Fig. 6. The DSC curves show a well-defined broad crystallization peak. The characteristic temperatures of the glass increased with the increase in heating rate. For studying the crystallization of the glasses by DSC analysis, one has to use DSC curves with well-defined crystallization peak. In addition, the glass must to be stable according to the parameter (T_c–T_g). So, in our study, the glass ($x = 0.1$) is chosen according to the above considerations. Table 2 shows the obtained crystallization temperature (T_c) for the glass ($x = 0.1$). A plot of $\ln(T_p^2/\beta)$ versus $1/T_p$ showed a straight line (Fig. 7), and from its slope the value of E_c can be determined. The value of E_c obtained is 232.67 kJ mol^{-1}. From the experimental DSC curves, the Avrami exponent, n, can also be obtained from the following equation [26]:

$$n = (2.5/\Delta T) \times \left(RT_p^2/E_c\right) \tag{4}$$

where ΔT is the width at half height of the crystallization peak. Applying the method developed by Avrami [27–29], the value calculated for n is very close to 1.7 (see Table 2), suggesting that surface crystallization is dominant during the crystallization of the glasses [30].

Infrared spectra of the glasses (IR)

Figure 8 shows the IR spectra of the $x\mathrm{Ba}_{0.5}\mathrm{Sr}_{0.5}\mathrm{TiO}_3$–$(1-x)\mathrm{NaPO}_3$ glasses. These spectra contain characteristic bands of the phosphate glasses. All the spectra are shifted for the sake of clearness. Each spectrum shows several absorption bands localized around 1279–1227, 1197–1155, 1094–1050, 1008-–994, 928–910, 755, 731, 632–623, 554 and 473 cm^{-1} (Table 3). The attribution of the absorption bands is done according to the literature assignments [27–39]. The characteristic vibrations of P–O bonds are included in broad band between 900 and 1300 cm^{-1}.

The absorption bands of the given materials can be assigned as follows: (1) the band at 1279–1227 cm^{-1} is due to the asymmetric stretch vibrations (P=O), and the band lying in the range 1197–1155 cm^{-1} is related to the

Table 3 Infrared band assignments in 1400–400 cm^{-1} range for $x\mathrm{Ba}_{0.5}\mathrm{Sr}_{0.5}\mathrm{TiO}_3$–$(1-x)\mathrm{NaPO}_3$ glasses

X	ν_{as} P=O/ν_{as}PO$_2^-$/ cm^{-1}	ν_{as} PO$_2^-$/ cm^{-1}	ν_s PO$_3^{2-}$/ cm^{-1}	ν_{as} PO$_4^{3-}$/ cm^{-1}	ν_{as} P–O–P/ cm^{-1}	ν_{as} P–O–P/ cm^{-1}	ν TiO$_4$/ cm^{-1}	ν TiO$_6$/ cm^{-1}	δ(PO$_4$)χμ^{-1}
0	1279	1197	1094	–	910	755	–	–	529/454
0.05	1235	1171	1089	1008	903	753	–	623	542/441
0.1	–	1166	1077	1000	924	–	731	627	549/473
0.15	1230	1155	1050	994	928	–	728	627	552/494
0.2	1227	–	–	–	–	–	729	632	555/491

stretching vibration of the $(PO_2)^-$ group [33, 39]; these bands are frequency decreasing when $NaPO_3$ content decreases; (2) the intensity of the band at $\approx 755\ cm^{-1}$, attributed to a stretching vibration of P–O–P bridges decreases with increasing $Ba_{0.5}Sr_{0.5}TiO_3$ content, but with further introduction of $Ba_{0.5}Sr_{0.5}TiO_3$, this band is replaced by two new bands one at 731 cm^{-1} and the other one in the region frequency 632–623 cm^{-1}. These new bands are assigned, respectively, to TiO_6 and TiO_4 structural units [40, 41]; (3) the band located in 1094–1050 cm^{-1} present in all the spectra is assigned to the high- and low-frequency components of the asymmetric stretch of the $(PO_3)^{2-}$ terminal group [33]. The increase in $Ba_{0.5}Sr_{0.5}TiO_3$ content induces the appearance of a broad band near 1008–994 cm^{-1} which is attributed to stretching vibration of the monophosphate PO_4 group. The broad bands around 554 and 473 cm^{-1} are associated with the bending vibrations of basic structural units of the phosphate network.

The significant bands detected in the region of 450–580, 650–800 and 900–1280 cm^{-1} are attributed to metaphosphate $(PO_3)^-$ and pyrophosphate $(P_2O_7)^{4-}$ units in accordance with functional groups of the crystalline phase identified by XRD: $NaPO_3$ (JCPDS 02-0436), $(NaPO_3)_6$ (JCPDS 48-0829), $Sr(PO_3)_2$ (JCPDS 89-6594), $Ba_2P_2O_7$ (JCPDS 09-0045) and $Sr_2P_2O_7$ (JCPDS 12-0362).

Conclusions

The glasses inside the $x$$Ba_{0.5}Sr_{0.5}TiO_3$–$(1-x)$$NaPO_3$ system were prepared by melt-quenching route, and their physical properties (density, T_g, H_v) increase with $Ba_{0.5}Sr_{0.5}TiO_3$ ratio. IR spectra indicate the formation of different phosphate units along with TiO_4 and TiO_6 groups in the glasses. The crystallization of the glasses is performed by heat treatments, and the obtained glass–ceramics contain sodium titanate Na_2TiO_3 (perovskite structure) phase rather than $Ba_{0.5}Sr_{0.5}TiO_3$ phase. The calculated values for the Avrami parameter (n) indicated that surface crystallization was the dominant crystallization mechanism.

Acknowledgements The authors would like to thank the Swedish Research Council for the financial support of this work.

References

1. Jones R, Zurcher P, Chu P, Taylor DJ, Lii YT, Jiang B, Maniar PD, Gillespie SJ. Memory applications based on ferroelectric and high-permittivity dielectric thin films. Microelectron Eng. 1995;29:3–10.
2. MuÈcklich F, Janocha H. Smart materials: the IQ of materials in systems. Z Metallkd. 1996;873:57–364.
3. Sinouh H, Bih L, Azrour M, ElBouari A, Benmokhtar S, Manoun B, Belhorma B, Baudin T, Berthet P, Haumont R, Solas D. Elaboration and structural characterization of glasses inside the ternary SrO-TiO_2-P_2O_5 system. J Phys Chem Solids. 2012;73:961–8.
4. Yadav AK, Gautam C. Successive relaxor ferroelectric behavior in La modified (Ba, Sr)TiO3 borosilicate glass ceramics. J Mater Sci Mater Electron. 2014;25:3532–6.
5. Herczog A. Microcrystalline $BaTiO_3$ by crystallization from glass. J Am Ceram Soc. 1964;47:107–15.
6. Ulrich DR. High dielectric thick films from screened circuit capacitors. Solid State Technol. 1969;12:30–8.
7. Sigaev VN, Sarkisov PD, Stefanovich SY, Pernice P, Aronne A. Glass ceramic textures based on new ferroelectric complex oxides. Ferroelectrics. 1999;233:165–85.
8. Houng B, Kim CY, Haun MJ. Densification, crystallization, and electrical properties of lead zirconate titanate glass-ceramics. IEEE T Ultrason Ferr. 2000;47:808–18.
9. Duan F, Fang C, Ding Z, Zhu H. Properties and applications of a piezoelectric glass-crystalline phase composite in the BaO–SrO–TiO_2–SiO_2 system. Mat Lett. 1998;34:184–7.
10. Lurie KA, Yakovlev VV. Method of control and optimization of microwave heating in waveguide systems. IEEE Trans Mag. 1999;35:1777–80.
11. Ruiz-Valdés JJ, Gorokhovsky AV, Escalante-Garcìa JI, Mendoza-Suárez G. Glass-ceramic materials with regulated dielectric properties based on the system BaO–PbO–TiO_2–B_2O_3–Al $_2O_3$. J Eur Ceram Soc. 2004;24:1505–8.
12. Shannon RD. Revised effective ionic radii and systematic studies of interatomic distances in halides and chalcogenides. Acta Crystallogr A. 1976;32:751–67.
13. Brow RK. Review: the structure of simple phosphate glasses. J Non-Cryst Solids. 2000;263–264:1–28.
14. Shaw CM, Shelby JE. Preparation and properties of stannous fluorophosphate glasses. Phys Chem Glasses. 1988;29:49–53.
15. Brow RK, Kirkpatrick RJ, Turner GL. Local structure of $xAl_2O_3\cdot(1-x)$ $NaPO_3$ glasses: an NMR and XPS study. J Am Ceram Soc. 1990;73:2293–300.
16. Donald IW. Preparation, properties and chemistry of glass- and glass-ceramic-to-metal seals and coatings. J Mater Sci. 1993;28:2841–86.
17. Sinouh H, Bih L, El Bouari A, Baudin T, Berthet P, Haumont R, Solas D. Glass and glass-ceramics along the $SrTiO_3$–$NaPO_3$ line. MATEC Web Conf. 2013;5:1–3.
18. Yamane M, Mackenzie JD. Vicker's hardness of glass. J Non-Cryst Solids. 1974;15:153–64.
19. Sinouh H, Bih L, El Bouari A, Azrour M, Manoun B, Lazor P. BaO effect on the thermal properties of the phosphate glasses inside the Na2O–SrO–TiO_2–B_2O_3–P_2O_5 system. J Phys Chem Solids. 2014;405:33–8.
20. Kissinger HE. Variation of peak temperature with heating rate in differential thermal analysis. J Res Natl Bur Stand. 1956;57:217–21.
21. Yinnon H, Uhlmann DR. Applications of thermoanalytical techniques to the study of crystallization kinetics in glass-forming liquids, part I: theory. J Non-Cryst Solids. 1983;54:253–75.
22. Aly KA, Saddeek YB, Dahshan A. Structure and crystallization kinetics of manganese lead tellurite glasses. J Therm Anal Calorim. 2015;119:1215–24.
23. Ivanović VDZ, Tosić MB, Grujić SR, Matijasević SD, Stojanović JN, Nikolić JD, Smiljanic SV. DTA study of the crystallization of Li_2O–Nb_2O_5–SiO_2–TiO_2 glass. J Therm Anal Calorim. 2015;119:1653–61.
24. Arya SK. Singh K, Thermal and kinetic parameters of $30Li_2O$–$55B_2O_3$–5ZnO–$xTiO_2$–$(10-x)V_2O_5$ glasses $(0 \leq x \leq 10)$. J Therm Anal Calorim. 2015;122:189–95.

25. Zemenová P, Kral R, Nitsch K, Knizek K, Cihlar A, Bystrický A. Characterization and crystallization kinetics of Er-doped Li_2O–Y_2O_3–P_2O_5 glass studied by non-isothermal DSC analysis. J Therm Anal Calorim. 2016;125:1431–8.
26. Augis JA, Bennett JE. Calculation of Avrami parameters for heterogeneous solid state reactions using a Modified Kissinger's method. J Therm Anal Calorim. 1978;13:283–92.
27. Avrami M. Kinetics of phase change. I General theory. J Phys Chem. 1939;7:1103–12.
28. Avrami M. Kinetics of phase change. II. Transformation-time relations for random distribution of nuclei. J Phys Chem. 1940;8:212–24.
29. Avrami M. Kinetics of phase change. III. Granulation, phase change, and microstructure. J Phys Chem. 1941;9:177–84.
30. Tosic MB, Dimitrijevic RZ, Mitrovic MM. The crystallization of calcium phosphate glass with the ratio $[CaO]/[P_2O_5]<1$. J Mater Sci. 2003;38:1983–94.
31. Higazy AA, Bridge B. Infrared spectra of the vitreous system Co_3O_4–P_2O_5 and their interpretation. J Mater Sci. 1985;20:2345–58.
32. Selvaraj LJ, Rao KJ. Role of lead in lead phosphomolybdate glasses and a model of structural units. J Non-Cyst Solids. 1988;104:300.
33. Efimov AM. IR fundamental spectra and structure of pyrophosphate glasses along the $2ZnO \cdot P_2O_5$–$2Me_2O \cdot P_2O_5$ join (Me being Na and Li). J Non-Cryst Solids. 1997;209:209–26.
34. Yung SW, Shih PY, Chin TS. Crystallization kinetics of a low melting PbO–ZnO–P_2O_5 glass. Mater Chem Phys. 1998;57:111–6.
35. Shih PY, Yung SW, Chin TS. FTIR and XPS studies of P_2O_5–Na_2O–CuO glasses. J Non-Cryst Solids. 1999;244:211–22.
36. Hudgens JJ, Martin SW. Glass transition and infrared spectra of low-alkali, anhydrous lithium phosphate glasses. J Am Ceram Soc. 1993;76:1691–6.
37. Meyer K. Structural characterisation of binary magnesium ultraphosphate glasses by vibrational spectroscopy. Phys Chem Glasses. 2001;42:79–87.
38. Metwalli E, Brow RK. Modifier effects on the properties and structures of aluminophosphate glasses. J Non-Cryst Solids. 2001;289:113–22.
39. Kamitsos EI, Kapoutsis JA, Chryssikos GD, Hutchinson JM, Pappin AJ, Ingram MD, Duffy JA. Infrared study of AgI containing superionic glasses. Phys Chem Glasses. 1995;36:141–9.
40. Laudisio D, Catauro M, Aronne A, Pernice P. Glass transition temperature and devitrification behaviour of lithium-titanium-germanate glasses. Thermochim Acta. 1997;294:173–8.
41. Wu HF, Lin CC, Shen P. Structure and dissolution of CaO–ZrO_2–TiO_2–Al_2O_3–B_2O_3–SiO_2 glass (II). J Non-Cryst Solids. 1997;209:76–86.